Structural and magnetic properties of epitaxial Fe/CoO bilayers on Ag(001)

R. Abrudan,[1,2] J. Miguel,[1,*] M. Bernien,[1] C. Tieg,[2,†] M. Piantek,[1] J. Kirschner,[2] and W. Kuch[1]
[1]*Institut für Experimentalphysik, Freie Universität Berlin, Arnimallee 14, D-14195 Berlin, Germany*
[2]*Max-Planck-Institut für Mikrostrukturphysik, Weinberg 2, D-06120 Halle, Germany*
(Received 31 July 2007; revised manuscript received 30 October 2007; published 10 January 2008)

We have investigated the magnetic coupling between a metallic ferromagnet and an oxidic antiferromagnet in epitaxial single-crystalline Fe/CoO bilayers on Ag(001) using x-ray absorption spectroscopy. Absorption spectra taken from bilayers with different amounts of deposited Fe show only a weak indication for the formation of Fe oxide at the Fe/CoO interface. From the spectral shape, it is concluded that an FeO type of oxide is formed. X-ray magnetic circular dichroism (XMCD) measurements exhibit a sizable induced ferromagnetic signal at the Co $L_{2,3}$ absorption edges, corresponding to an interface layer of 1.1 ML of CoO in which the Co magnetic moments couple with the Fe moments. The angular dependence of the Fe XMCD and Co x-ray magnetic linear dichroic signals at the $L_{2,3}$ edges shows that the orientation of the Co and Fe spins is parallel along the crystallographic ⟨110⟩ directions.

DOI: 10.1103/PhysRevB.77.014411 PACS number(s): 68.55.−a, 75.50.Ee, 75.70.−i, 78.70.Dm

I. INTRODUCTION

Since the discovery of the exchange-bias effect by Meiklejohn and Bean[1] in the 1950s, work in the field of magnetic coupling phenomena between a ferromagnetic (FM) and an antiferromagnetic (AFM) material has focused on the role of the FM/AFM interface. Systems such as oxide-coated particles, e.g., CoO/Co,[1] mono- and polycrystalline ferromagnets deposited on bulk oxides,[2] and thin-film bi- and trilayers,[3,4] have been studied and extensive theoretical work[5–8] has been carried out trying to puzzle out the exchange-bias mechanism.

Despite this effort, a complete picture of the exchange-bias mechanism is not yet evident, since it also involves the understanding of the FM/AFM interface not only from the structural point of view but also electronically and magnetically. A general theory of the interface cannot be presented because of its complexity and numerous ingredients such as roughness, strain effects between layers,[3] spin rotation of the AFM near the interface,[9] or layer thickness.[10]

It is at the FM/AFM interface where the AFM spins of the last layer are not fully compensated by their neighbors, so that they may couple to the FM layer. The so-called uncompensated AFM spins play a key role in the exchange-bias process and have been identified as the origin of the exchange-bias field,[11] the increase in the coercive field of the FM layer,[12] and training effects.[13,14] Depending on the particular materials involved and on the specific microstructure, they might be parallelly[15] or antiparallelly[16–19] coupled to the FM layer, or even both.[20]

Due to their element and chemical specificities, synchrotron-based techniques such as x-ray absorption spectroscopy (XAS) with the magnetic circular[21–23] and linear[24] dichroic effects, x-ray photoelectron emission microscopy,[25] and x-ray resonant magnetic scattering[26] are extremely powerful techniques for studying FM/AFM interfaces. They have provided vital information on the interfacial properties,[2,27–30] revealing, for example, the presence of AFM spins coupled ferromagnetically to the FM layer at the interface.[28]

Recent experiments had revealed that for CoO films grown on different substrates, a strong dependence exists between the magnitude and orientation of the magnetic moments and the substrate-induced strain in the system.[3] A CoO film sandwiched by MnO layers shows an out-of-plane spin axis, but when in direct contact with the Ag(001) substrate, the spins are in plane.

In this paper, we focus on the properties of ultrathin Fe/CoO bilayers grown onto Ag(001), which were studied by means of polarization-dependent XAS at the Fe and Co $L_{2,3}$ edges ($2p$-$3d$ transitions). The transition-metal–oxide CoO, like its equivalents MnO and NiO, forms an antiferromagnetic, rocksalt crystal structure in such a way that two transition-metal (TM) electrons occupy the O $2p$ shell leading to an O^{2-} ion and a TM^{2+} ion. The antiferromagnetic order of bulk CoO is a type-II antiferromagnet: following the [100] direction of the face-centered-cubic (fcc) lattice, the Co spins (separated by oxygen atoms) are coupled antiferromagnetically. Furthermore, within the {111} planes, the spins are parallel, whereas moments of neighboring {111} planes have their spins antiparallelly aligned to the previous ones. In the case of bulk CoO, accompanying the paramagnetic-antiferromagnetic transition at the Néel temperature $T_N = 289$ K,[31] the system also undergoes a crystallographic phase change from a cubic lattice structure to a monoclinic one.[32]

In order to investigate the effect of these strain-induced changes of the CoO spin direction on the Fe magnetization, well-defined interfaces are needed. Hence, we have studied epitaxially deposited thin Fe/CoO films on Ag(001) by means of x-ray magnetic circular dichroism (XMCD) and x-ray magnetic linear dichroism (XMLD). These techniques allow us to determine the orientation of the magnetic spin axis in both layers and to study in detail the chemical and magnetic characters of the interface.

II. EXPERIMENT

The experiments were performed in ultrahigh vacuum chambers equipped with facilities for growth, structural, and magnetic characterizations of samples. The sample can be rotated about both the polar (θ) and azimuthal (ϕ) axes with

1° and 5° accuracies, respectively. A Ag(001) single crystal was used as a substrate, which was cleaned by Ar^+ sputtering (750 eV) successively at 300 and 380 K, followed by annealing at 750 K for 10 min. The sputter-anneal sequence was repeated until the low energy electron diffraction (LEED) image showed sharp (1×1) spots.

Starting from a base pressure of 3×10^{-10} mbar in the preparation chamber, CoO layers were prepared by electron-beam evaporation of Co (purity of 99.99%) in an oxygen atmosphere of 1.3×10^{-6} mbar. In order to avoid precursor formation with different crystallographic orientations[33] and to improve the Co oxidation at the surface, the Ag(001) substrate was kept at 450 K during the deposition. Postannealing of the CoO/Ag(001) films was done under oxygen atmosphere (10^{-6} mbar) for 30 min at $T=750$ K. The Fe layer was deposited onto the CoO film at room temperature. The deposition rates for Fe and Co were 1 and 0.5 ML/min, respectively. The slower Co deposition ensured a complete oxidation and avoided cluster formation on the Ag(001) surface. Layer thicknesses were checked by means of Auger electron spectroscopy and the XAS edge jump intensities. LEED patterns provided information on the in-plane structure of the CoO film. We used a kinematic theory[34–38] to analyze the energy dependence of the (00) LEED spot intensity in order to obtain information about the average vertical interlayer distance.

In situ thickness- and temperature-dependent magneto-optical Kerr effect (MOKE) measurements in longitudinal geometry were performed to study the magnetism of the bilayer system with the external magnetic field applied along the [110] direction of the substrate, i.e., along the [100] Fe magnetization easy axis.

X-ray absorption spectroscopy experiments with total electron yield detection were performed at beamline UE56/2-PGM2 at BESSY. We used this undulator and plane grating monochromator beamline to produce circularly and linearly polarized photons with an energy resolution of about 100 meV in the 650–850 eV energy range. The measurements were done in magnetic remanence after saturating the samples in a magnetic field of 32 kA/m applied along the [110] direction of the substrate. The spectra were normalized to the incoming photon flux using the drain current from the last refocusing mirror before the measuring chamber. Unless indicated in the text, the spectra were then normalized to zero and 1 in the pre- and postedge energy regions, respectively.

In order to study separately the magnetization of both layers, different measurement geometries were used. The Fe $L_{2,3}$ XMCD signal was measured using left and right circularly polarized light at grazing incidence, with an angle $\theta=70°$ between the wave vector **k** and the surface normal **n**, as shown in Fig. 1(a). Since it is a direct measure of the expectation value of the magnetization $\langle\mathbf{M}\rangle$, XMCD was employed to determine the direction of magnetic moments in the ferromagnetic Fe layer.

The linear dichroism effect probes the anisotropy of the local charge density distribution in the system.[39] In contrast to XMCD, XMLD spectroscopy measures the expectation value of the magnetization squared $\langle\mathbf{M}^2\rangle$,[40] so that it can only determine the orientation of the spin axis. The geometry used in this case is shown in Fig. 1(b).

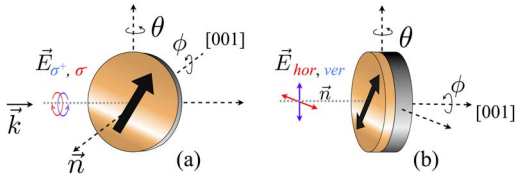

FIG. 1. (Color online) Experimental geometries used for the x-ray absorption measurements. The angle θ is defined as the angle between the surface normal **n** and the **k** vector of the light. ϕ is the angle between the [100] crystal axis of the substrate and the **E** vector of horizontally polarized light. (a) Geometry for XMCD measurements, with the sample at grazing incidence ($\theta=70°$), and (b) geometry for XMLD experiments.

III. RESULTS AND DISCUSSION

A. Growth and structural studies

Figure 2 shows the LEED patterns of a clean Ag(001) surface [panel (a)] and of a 9 ML CoO film on Ag(001) prepared as described in Sec. II [panel (b)]. To illustrate the effect of the substrate temperature on the quality of the CoO layer, we show the corresponding LEED patterns for 10 ML CoO grown on Ag(001) at 300 K (c) and at 450 K and after annealing at 750 K for 30 min (d). The clear improvement in the spot sharpness confirms the better quality in the second case. From these LEED results, we conclude that ultrathin CoO layers on Ag(001) keep the in-plane fcc structure from the bulk.

The LEED-$I(E)$ curves of the specular (00) spot of the clean Ag(001) substrate and those of CoO/Ag(001) samples of different film thicknesses are shown in Fig. 2(e). From the evolution of the energies and intensities of the three peaks labeled as 4, 5, and 6, we calculate an average interlayer distance $a/2=2.17$ Å for thicknesses below 10 ML. Direct comparison with the bulk value ($a/2=2.13$ Å) evidences a vertical expansion of the oxide in the thin-film regime.

In order to check if the predicted crystallographic monoclinic distortion of the bulk CoO below T_N (Ref. 32) is also evident in the ultrathin-film regime, low-temperature LEED measurements were carried out, showing no difference when compared to the room-temperature images.

Upon evaporation of Fe at room temperature, the corresponding LEED image (not shown) proves the epitaxial growth of Fe onto the CoO layer. Since the bcc Fe unit cell is rotated by 45° with respect to the CoO unit cell, the ⟨100⟩ Fe easy magnetic axes correspond to the ⟨110⟩ substrate crystal directions.

B. Magnetism

Figure 3 shows the temperature dependence of the Fe coercive field for several CoO thicknesses extracted from MOKE loops. The CoO thickness ranged from 3 to 10 ML, whereas the Fe thickness was kept constant at 7 ML. The samples were cooled in zero magnetic field from the as-

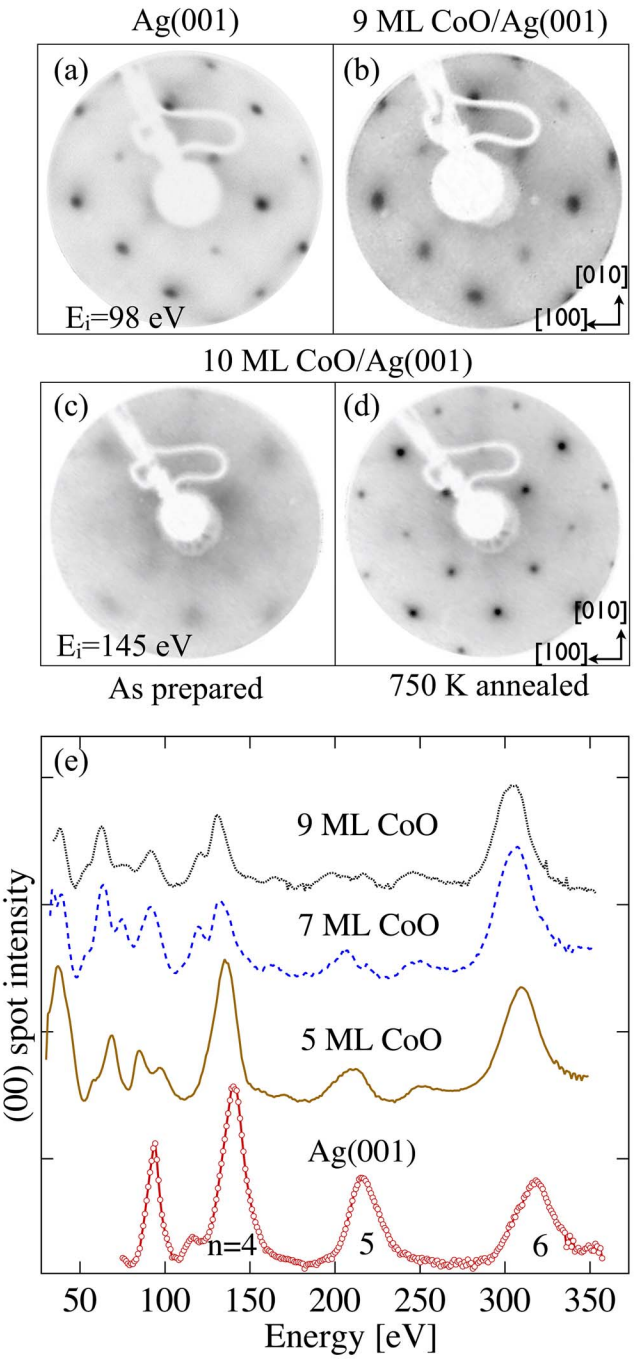

FIG. 2. (Color online) LEED patterns for (a) the clean Ag(001) substrate, (b) CoO(9 ML)/Ag(001), and CoO(10 ML)/Ag(001) (c) as prepared and (d) after annealing. (e) Energy dependence of the LEED (00) spot intensity for CoO films grown on Ag(001). $I(E)$ curves are obtained at $\theta=5°$ electron incidence with respect to the surface normal.

grown state; thus, no hysteresis loop shift was present. However, a clear increase in the coercive fields is visible for all CoO thicknesses at temperatures lower than 293 K, when the antiferromagnetic order is established. Beyond that point, steeper slopes are observed for thicker CoO layers, indicating that the magnetic losses[57] of the CoO layer increase with

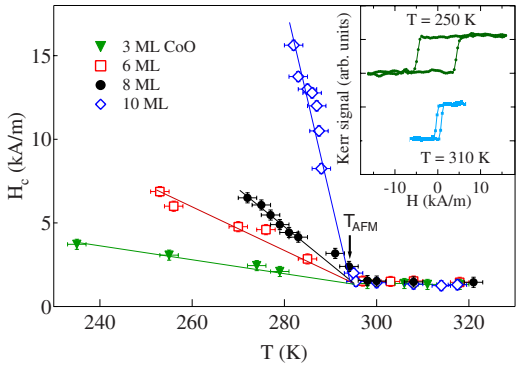

FIG. 3. (Color online) Temperature dependence of the coercive field H_c of the 7 ML Fe layer for different CoO underlayer thicknesses (lines are guides to the eye). The inset shows typical MOKE hysteresis loops for $t_{CoO}=6$ ML.

the thickness, although the coercivity enhancement as a function of thickness is not yet saturated for 10 ML CoO. Furthermore, the resulting ordering temperature for thin films roughly agrees with the bulk Néel temperature $T_N=290$ K. Similar values have been found for sputtered CoO/Fe bilayers[4] ($T_{AFM}=289$ K) and on evaporated CoO thin layers on Ag(001) and MnO/Ag(001) (Ref. 3) ($T_{AFM}=310$ K).

C. Spectroscopy

Linear dichroic effects may have structural and magnetic origins, which can be separated by measuring at temperatures higher than T_{AFM}. Figure 4(a) shows the room-temperature XA spectra obtained for 10 ML CoO/Ag(001) with horizontally polarized light and polar angles $\theta=0°$, 45°, and 70°. The spectra were corrected for saturation effects present when measuring at grazing angles.[41] The difference spectrum between the normal and grazing XA spectra [displayed in Fig. 4(b)] shows a strong linear dichroism. We attribute this effect to the tetragonal distortion of the unit cell caused by the vertical lattice expansion of the film, as described above. At normal incidence, no linear dichroism was

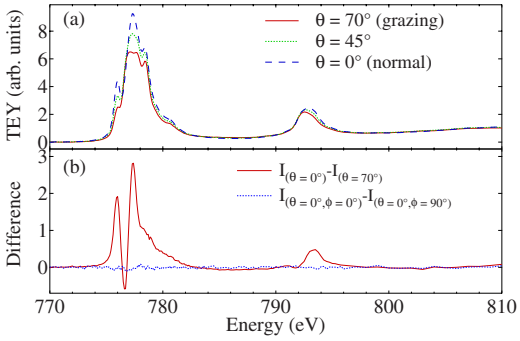

FIG. 4. (Color online) (a) XA spectra of CoO(10 ML)/Ag(001) for $\theta=0°$, 45°, and 70° at room temperature. (b) X-ray linear dichroic (XLD) spectrum obtained as $I_{(\theta=0°)}-I_{(\theta=70°)}$ (full line). The dotted line shows the XLD at normal incidence under a 90° rotation of the sample about the surface normal.

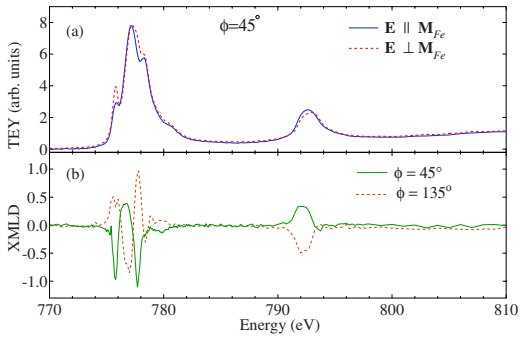

FIG. 5. (Color online) Co $L_{2,3}$ (a) XAS and (b) XMLD spectra for Fe(6 ML)/CoO(10 ML)/Ag(001) recorded with **E** parallel (full line) and perpendicular (dashed line) to $\mathbf{M}_{\mathrm{Fe}}$ at 150 K (θ=0°, ϕ =45°). The dashed line in (b) is the XMLD signal for ϕ=135°.

found between ϕ=0° and 90° [Fig. 4(b), dotted line], which indicates the absence of any in-plane distortion in the CoO unit cell for this thickness range. The structural dichroism here is much larger than the one observed in a similar system,[3] probably because the films are more epitaxial and thus more strained in our case.

On the other hand, a large magnetic linear dichroic signal was found on a 6 ML Fe/10 ML CoO/Ag(001) sample after applying a saturating magnetic field **H**=32 kA/m along the [110] substrate crystallographic direction and cooling down to 150 K. Figure 5(a) shows the two Co $L_{2,3}$ XA spectra measured with **E** parallel to [110] (full line) and perpendicular to it (dashed line). The corresponding XMLD signal [full line in panel (b)] comprises a negative-positive-negative succession of sharp peaks at E=775.8, 776.6, and 777.7 eV (L_3 edge) and a single broader positive peak centered around 792.0 eV (L_2 edge). The asymmetry values for these energies, defined as $A=(I_v-I_h)/(I_v+I_h)$, are A=−14.1%, 3.8%, −8.8%, and 7.0%, respectively. All the spectral features found in the XAS and XMLD line shapes are in good agreement with literature results on 8 ML CoO/NiO(100),[42] where no in-plane or out-of-plane lattice distortion was mentioned. By the sign inversion of the XMLD signal for ϕ =135° (dashed line), we prove the twofold symmetry of the CoO antiferromagnetic order.

Recent results on Fe_3O_4 (Ref. 43) and NiO (Ref. 44) have stressed the relevance that the spin orientation, relative to the crystallographic directions, has on the XMLD signals. In a system with octahedral crystal field symmetry, any XMLD spectrum can be formed by a linear combination of two fundamental spectra I_0 and I_{45}, not just one as it was previously used.[45] The authors of Ref. 44 represented the XMLD signal observed as the difference of spectra with **E** parallel and perpendicular to **M**, for $\mathbf{M}\|[100]$ (I_0) and $\mathbf{M}\|[110]$ (I_{45}), and compared them to atomic multiplet calculations.[46] In particular, it was found that the Ni L_2 XMLD signal reverses sign when the AFM NiO spin axis is turned from the ⟨100⟩ to the ⟨110⟩ crystallographic directions[44] [$I_{45}(L_2)\approx -I_0(L_2)$]. Thus, it was concluded that the coupling between the Co and NiO layers is perpendicular, in contrast to previous publications.[28] The same sign inversion at the respective L_2 edge has been observed[47] for Mn^{2+}. In all these cases, the L_2 sign inversion seems to be a much more robust feature than the shape of the L_3 edge, where slightly different features appear in the $I_{0,45}$ spectra.

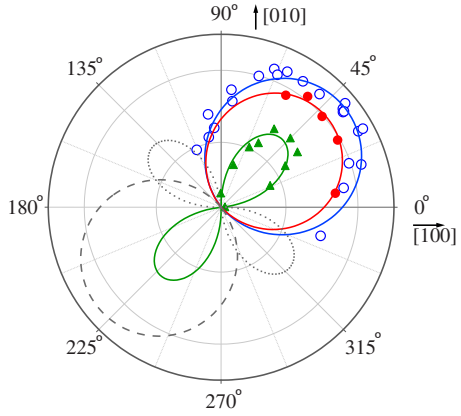

FIG. 6. (Color online) Azimuth-angle dependence of the Fe XMCD and Co XMLD signals. Full and open circles represent the Fe L_3 XMCD signal at 150 and 300 K, respectively; full triangles represent the measured Co L_2 XMLD signal (5×). Lines are the best fits to functions, as described in the text, where the dashed and dotted sections are for opposite signs of the XMLD and XMCD, respectively.

In our case, it is observed that the Co spin axis in the CoO layer below T_{AFM} is along the ⟨110⟩ directions, either parallel or perpendicular to $\mathbf{M}_{\mathrm{Fe}}$, but in any case described by I_{45}. Unfortunately, up to date, they are only calculations available for the Co I_0 XMLD spectrum in an O_h crystal field.[58] We will therefore assume a similar sign inversion between I_0 and I_{45} at the Co L_2 edge to discuss the coupling direction in the Fe/CoO system.

The calculated I_0 spectrum for Co^{2+} displays a negative peak at the L_2 edge, with a small positive shoulder at the right-hand side of the peak. Our experimental CoO XMLD signal [shown in Fig. 5(b)] resembles rather well these features but with the opposite sign. From this sign reversal, we infer that our XA spectra for horizontal polarization corresponds to parallel alignment of **E** and the AFM spin axis. Therefore, we conclude that there is a collinear coupling between the Fe magnetization and the CoO spin axis.

Focusing now on the azimuthal and temperature dependences of the dichroic signals, we probe the evolution of the Fe magnetization and the magnetic coupling of the two layers. Figure 6 shows a polar plot of the Fe L_3 XMCD and Co L_2 XMLD vs ϕ, measured at grazing and normal incidences, respectively. The full lines show best fits of the XMCD and XMLD data to $\sin(\phi+\phi_{\mathrm{Fe}})$ and $\sin[2(\phi+\phi_{\mathrm{Co}})]$ functions. The dashed and dotted lines are the extrapolations of the fits for opposite sign. From the fitting of the Fe XMCD at 300 K, a $\phi_{\mathrm{Fe}}(\mathrm{RT})$=44.3° angle between $\mathbf{M}_{\mathrm{Fe}}$ and the [100] axis of the substrate is obtained, as expected. After the zero-field cooling, at remanence, the Fe magnetic easy direction does not change [$\phi_{\mathrm{Fe}}(\mathrm{LT})$=42.5°], agreeing within the error bars with the MOKE results described in Sec. II. However, a small decrease in the XMCD intensities is observed, which can be explained by a partial breaking up into domains or by a canting of the Fe magnetization concomitant to the devel-

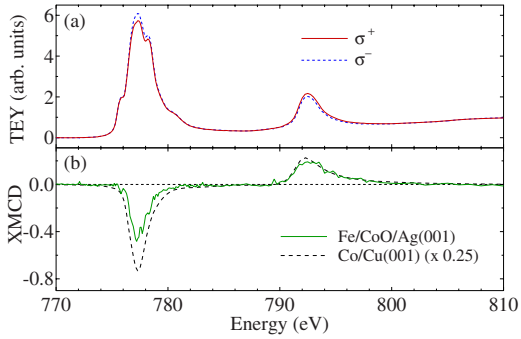

FIG. 7. (Color online) (a) Co $L_{2,3}$ XA spectra from Fe(6 ML)/CoO(10 ML)/Ag(001) measured at grazing incidence with left (σ^+) and right (σ^-) circular polarizations; (b) the corresponding XMCD difference spectrum (full line) and the one measured on Co(10 ML)/Cu(001) (dashed line). For the sake of a better comparison, the metallic XMCD difference was scaled ($0.25\times$) to match the L_2 edge.

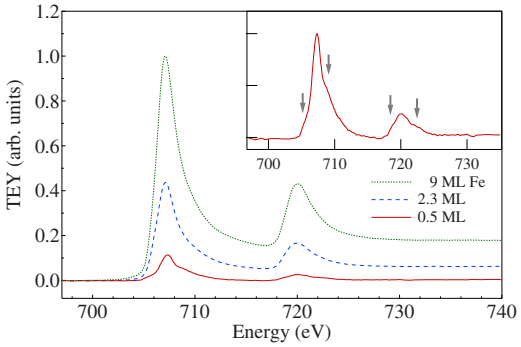

FIG. 8. (Color online) XA spectra for different thicknesses of Fe deposited on 8 ML CoO/Ag(001). The inset shows the zoomed-in spectrum for 0.5 ML Fe/8 ML CoO/Ag(001); the oxidic shoulders on each peak side are emphasized by arrows.

opment of the CoO antiferromagnetic order. A similar reduction of the XMCD signal after cooling an AFM/FM system has been observed in NiCoO/Co.[48] Upon field cooling (data not shown), the Fe XMCD signal is seen to recover the room-temperature value.

Furthermore, the azimuthal dependence of the XMLD signals leads to a $\phi_{Co}=47.9°$ angle between the CoO spins and the [100] crystal direction. Based on our earlier discussion on the sign of the XMLD, we interpret this as collinear coupling of $\mathbf{M}_{Fe}$ and the CoO spin axis, in this case along the ⟨110⟩ crystallographic axes. In an almost fully compensated FM/AFM interface, a 90° coupling is the energetically preferable[49] and is the case for Co/NiO.[44] In our case, the collinear coupling is the result of the common preferable orientations of the Fe magnetization and CoO spin axis along the ⟨110⟩ directions of the substrate and of the large amount of uncompensated Co spins at the interface, as will be discussed below. A more exotic 45° coupling is present in Co/FeMn,[50] caused by the noncollinear $3Q$ spin structure in the FeMn film.

The presence of CoO spins ferromagnetically coupled to the Fe layer has also been studied. Figure 7(a) shows the Co $L_{2,3}$ XA spectra for left and right circularly polarized light measured at grazing incidence and $\phi=45°$ at 150 K, whereas panel (b) shows the XMCD difference signal. Since no dichroism was found on CoO/Ag(001) under the same conditions, we infer that this XMCD signal is completely linked to the magnetization of the Fe layer. Assuming the presence of uncompensated Co spins with magnetic moments similar to metallic Co only at the interface, the considerably large Co XMCD asymmetry $[A(L_3)\approx 3.1\%]$ corresponds to about 1.1 ML uncompensated Co spins. For this calculation, we have assumed a secondary electron information depth of 2 nm and we have made use of the Co L_3 XMCD intensity of an fcc 10 ML Co/Cu(001) layer[51] $[A(L_3)\approx 18\%]$, the spectrum of which is also shown in Fig. 7(b) (dashed line). For a nominally compensated surface of the CoO, such a large amount of interfacial uncompensated Co spins at the interface supports the collinear coupling between Fe and CoO spin axes. Similar effects have been observed in Co/FeMn,[52] CoO/Fe,[4] and Co/NiO (Ref. 28) systems, where 0.75 ML uncompensated Ni spins was found.

The smaller branching ratio[53] of the CoO XMCD spectrum indicates a much larger orbital moment $\langle L_z\rangle$ of those spins, compared to the metallic Co case. It is also interesting to observe that the four main peak features of the CoO XA spectrum are reproduced in the XMCD difference signal, indicating that the uncompensated Co spins retain mainly their oxidic character.

In order to probe the extent of oxidation of the Fe layer at the interface, XA spectra were recorded for Fe layers with increasing thicknesses deposited on a freshly prepared 8 ML CoO/Ag(001) film. In order to stress the spectral features, these spectra (shown in Fig. 8) have not been normalized to the same edge jump. The energy shift of the Fe L_3 edge with respect to the ionic value is an excellent tool to ascertain the Fe oxidation state. It has been experimentally determined as $\Delta E=0$ and 1.4 eV for FeO and Fe_3O_4, respectively.[2] The only evidence of Fe oxidation can be seen in the case of 0.5 ML Fe thickness (enlarged in the inset). The energy position of those shoulders (indicated by arrows), together with the absence of an Fe L_3 energy shift, indicates the presence of FeO (rather than Fe_3O_4) at the interface. The additional shoulders could also come from the more atomic character of the Fe atoms,[54] depending on how they grow on top of the CoO layer. However, the atomiclike Fe L_2 XAS line shape in Ref. 54 does not show any additional shoulder, contrary to the measured 0.5 ML Fe XA spectrum, excluding atomiclike Fe atoms as the main origin for the observed spectral features.

The same type of oxidation was found in Fe/NiO bilayers.[2] By using a similar analysis of the relative peak intensities, we calculate the FeO thickness to be 0.3 ML. This is quite small compared to other studies on Fe/NiO systems[2,55] and may be explained by the smaller redox potential of Co compared to that of Ni. From this point of view, the Fe/CoO is a more suitable system to study the FM/AFM coupling mechanisms.

IV. CONCLUSIONS

A thorough structural and magnetic study of ultrathin epitaxial Fe/CoO FM/AFM systems has been carried out by

means of LEED, MOKE, XMCD, and XMLD. The vertical distortion of the CoO layers found by LEED-$I(E)$ results in an appreciable linear dichroism between spectra for normal and grazing incidences above the AFM ordering temperature. At normal incidence and low temperatures, the azimuth-dependent linear dichroism of the CoO layer is of pure magnetic origin and shows a collinear coupling of the CoO spin axis with the Fe magnetization along the $\langle 110 \rangle$ in-plane substrate directions, which coincides with the Fe [100] direction.

The presence of the Fe layer on top of the CoO layer pins the direction of some Co spins at the interface, leading to a sizable XMCD signal at the Co $L_{2,3}$ edge. Assuming a fully saturated spin moment, a thickness of 1.1 ML is estimated from XMCD for this layer of uncompensated spins. The XMCD spectrum also indicates that the Co atoms at the interface retain their oxidic character. Furthermore, a 0.3 ML FeO layer is observed at the Fe/CoO interface, independent of the total Fe thickness.

*miguel@physik.fu-berlin.de
†European Synchrotron Radiation Facility, BP 220, F-38043 Grenoble, France.

[1] W. H. Meiklejohn and C. P. Bean, Phys. Rev. **102**, 1413 (1956).
[2] T. J. Regan, H. Ohldag, C. Stamm, F. Nolting, J. Lüning, J. Stöhr, and R. L. White, Phys. Rev. B **64**, 214422 (2001).
[3] S. I. Csiszar, M. W. Haverkort, Z. Hu, A. Tanaka, H. H. Hsieh, H.-J. Lin, C. T. Chen, T. Hibma, and L. H. Tjeng, Phys. Rev. Lett. **95**, 187205 (2005).
[4] F. Radu, M. Etzkorn, R. Siebrecht, T. Schmitte, K. Westerholt, and H. Zabel, Phys. Rev. B **67**, 134409 (2003).
[5] J. S. Kouvel, C. D. Graham, and I. S. Jacobs, J. Phys. Radium **20**, 198 (1959).
[6] J. S. Kouvel and J. C. D. Graham, J. Appl. Phys. **30**, S312 (1959).
[7] A. P. Malozemoff, Phys. Rev. B **35**, 3679 (1987).
[8] N. C. Koon, Phys. Rev. Lett. **78**, 4865 (1997).
[9] F. Nolting *et al.*, Nature (London) **405**, 767 (2000).
[10] W. Kuch, L. I. Chelaru, K. Fukumoto, F. Porrati, F. Offi, M. Kotsugi, and J. Kirschner, Phys. Rev. B **67**, 214403 (2003).
[11] W. H. Meiklejohn and C. P. Bean, Phys. Rev. **105**, 904 (1957).
[12] W. J. Antel, F. Perjeru, and G. R. Harp, Phys. Rev. Lett. **83**, 1439 (1999).
[13] L. Malkinski, T. O'Keevan, R. E. Camley, Z. Celinski, L. Wee, R. L. Stamps, and D. Skrzypek, J. Appl. Phys. **93**, 6835 (2003).
[14] A. Hoffmann, Phys. Rev. Lett. **93**, 097203 (2004).
[15] H. Ohldag, A. Scholl, F. Nolting, E. Arenholz, S. Maat, A. T. Young, M. Carey, and J. Stöhr, Phys. Rev. Lett. **91**, 017203 (2003).
[16] J. Nogués, D. Lederman, T. J. Moran, and I. K. Schuller, Phys. Rev. Lett. **76**, 4624 (1996).
[17] A. Hoffmann, J. W. Seo, M. R. Fitzsimmons, H. Siegwart, J. Fompeyrine, J.-P. Locquet, J. A. Dura, and C. F. Majkrzak, Phys. Rev. B **66**, 220406(R) (2002).
[18] S. Roy *et al.*, Phys. Rev. Lett. **95**, 047201 (2005).
[19] E. Arenholz, K. Liu, Z. Li, and I. K. Schuller, Appl. Phys. Lett. **88**, 072503 (2006).
[20] H. Ohldag, H. Shi, E. Arenholz, J. Stöhr, and D. Lederman, Phys. Rev. Lett. **96**, 027203 (2006).
[21] C. T. Chen, Y. U. Idzerda, H. J. Lin, N. V. Smith, G. Meigs, E. Chaban, G. H. Ho, E. Pellegrin, and F. Sette, Phys. Rev. Lett. **75**, 152 (1995).
[22] J. Stöhr and R. Nakajima, IBM J. Res. Dev. **42**, 73 (1998).
[23] J. Stöhr, J. Magn. Magn. Mater. **200**, 470 (1999).
[24] G. van der Laan, B. T. Thole, G. A. Sawatzky, J. B. Goedkoop, J. C. Fuggle, J.-M. Esteva, R. Karnatak, J. P. Remeika, and H. A. Dabkowska, Phys. Rev. B **34**, 6529 (1986).
[25] F. Offi, W. Kuch, and J. Kirschner, Phys. Rev. B **66**, 064419 (2002).
[26] J. Miguel, J. F. Peters, O. M. Toulemonde, S. S. Dhesi, N. B. Brookes, and J. B. Goedkoop, Phys. Rev. B **74**, 094437 (2006).
[27] S. Altieri, L. H. Tjeng, and G. A. Sawatzky, Thin Solid Films **400**, 9 (2001).
[28] H. Ohldag, T. J. Regan, J. Stöhr, A. Scholl, F. Nolting, J. Lüning, C. Stamm, S. Anders, and R. L. White, Phys. Rev. Lett. **87**, 247201 (2001).
[29] W. Kuch, L. I. Chelaru, F. Offi, J. Wang, M. Kotsugi, and J. Kirschner, Nat. Mater. **5**, 128 (2006).
[30] J. Camarero, J. Miguel, J. B. Goedkoop, J. Vogel, F. Romanens, S. Pizzini, F. Garcia, J. Sort, B. Dieny, and N. B. Brookes, Appl. Phys. Lett. **89**, 232507 (2006).
[31] M. D. Rechtin and B. L. Averbach, Phys. Rev. B **6**, 4294 (1972).
[32] W. Jauch, M. Reehuis, H. J. Bleif, F. Kubanek, and P. Pattison, Phys. Rev. B **64**, 052102 (2001).
[33] R. Shantyr, Ph.D. thesis, Universität Halle-Wittemberg, 2004.
[34] J. B. Pendry, *Low Energy Electron Diffraction*, Techniques of Physics (Academic, London, 1974).
[35] W. Kuch, A. Dittschar, K. Meinel, M. Zharnikov, C. M. Schneider, J. Kirschner, J. Henk, and R. Feder, Phys. Rev. B **53**, 11621 (1996).
[36] C. Tieg, W. Kuch, S. G. Wang, and J. Kirschner, Phys. Rev. B **74**, 094420 (2006).
[37] M. Zharnikov, A. Dittschar, W. Kuch, C. M. Schneider, and J. Kirschner, J. Magn. Magn. Mater. **174**, 40 (1997).
[38] W. Kuch, F. Offi, L. I. Chelaru, M. Kotsugi, K. Fukumoto, and J. Kirschner, Phys. Rev. B **65**, 140408(R) (2002).
[39] S. S. Dhesi, G. van der Laan, and E. Dudzik, Appl. Phys. Lett. **80**, 1613 (2002).
[40] J. Stöhr, A. Scholl, T. J. Regan, S. Anders, J. Lüning, M. R. Scheinfein, H. A. Padmore, and R. L. White, Phys. Rev. Lett. **83**, 1862 (1999).
[41] R. Nakajima, J. Stöhr, and Y. U. Idzerda, Phys. Rev. B **59**, 6421 (1999).
[42] N. Weber, Ph.D. thesis, Heinrich-Heine-Universität Düsseldorf, 2001.
[43] E. Arenholz, G. van der Laan, R. V. Chopdekar, and Y. Suzuki, Phys. Rev. B **74**, 094407 (2006).
[44] E. Arenholz, G. van der Laan, R. V. Chopdekar, and Y. Suzuki, Phys. Rev. Lett. **98**, 197201 (2007).
[45] D. Alders, L. H. Tjeng, F. C. Voogt, T. Hibma, G. A. Sawatzky, C. T. Chen, J. Vogel, M. Sacchi, and S. Iacobucci, Phys. Rev. B **57**, 11623 (1998).
[46] R. D. Cowan, *The Theory of Atomic Structure and Spectra* (Uni-

versity of California Press, Berkeley, 1981).
[47] A. A. Freeman, K. W. Edmonds, G. van der Laan, N. R. S. Farley, T. K. Johal, E. Arenholz, R. P. Campion, C. T. Foxon, and B. L. Gallagher, Phys. Rev. B **73**, 233303 (2006).
[48] S. Brück, E. Goering, Y. J. Tang, G. Schütz, and A. E. Berkowitz, J. Magn. Magn. Mater. **310**, 2316 (2007).
[49] T. C. Schulthess and W. H. Butler, Phys. Rev. Lett. **81**, 4516LP (1998).
[50] W. Kuch, L. I. Chelaru, F. Offi, J. Wang, M. Kotsugi, and J. Kirschner, Phys. Rev. Lett. **92**, 017201 (2004).
[51] C. Tieg, Ph.D. thesis, Universität Halle-Wittemberg, 2006.
[52] F. Offi, W. Kuch, L. I. Chelaru, K. Fukumoto, M. Kotsugi, and J. Kirschner, Phys. Rev. B **67**, 094419 (2003).
[53] G. van der Laan and B. T. Thole, Phys. Rev. B **42**, 6670 (1990).
[54] P. Gambardella, S. S. Dhesi, S. Gardonio, C. Grazioli, P. Ohresser, and C. Carbone, Phys. Rev. Lett. **88**, 047202 (2002).
[55] P. Luches, V. Bellini, S. Colonna, L. Di Giustino, F. Manghi, S. Valeri, and F. Boscherini, Phys. Rev. Lett. **96**, 106106 (2006).
[56] G. van der Laan and B. T. Thole, Phys. Rev. B **43**, 13401 (1991).
[57] These magnetic losses can be understood in terms of the field needed either to twist the spin structure of the AFM layer or to move eventual domain walls during the reversal process.
[58] See Co^{2+} XMLD curve for $z=1$, $\Delta=1$ in Ref. 56.